Supplementary Information (SI) for Sustainable Energy & Fuels.
This journal is © The Royal Society of Chemistry 2026

Supplementary Information

Initial Temperature Regulated Precursor Solution Assembly Enables High Performance Organic Solar Cells

Xinyu Pu[a], Qifa Zheng[b], Zhenye Li[*a], Hanjian Lai[*a]

[a]College of Mechanical Engineering & School of Electrical Engineering, University of South China, Hengyang 421001, China

[b]Hunan Zhongyuan Technology Co., Ltd, Yanfeng District, Hengyang 421001, China

*Correspondence should be addressed to Z. L. and H. L.

Email: lizhenye@usc.edu.cn, and laihj@usc.edu.cn

Experimental

1. Materials

In this work, the polymer donor PM6 and the non-fullerene acceptor L8-BO were employed as the active-layer materials. The device architecture was ITO/PEDOT:PSS/active layer/PFN-Br/Ag. All solvents, interfacial materials, and other reagents used in the experiments were commercially available analytical-grade or electronic-grade products and were used as received without further purification.

2. Preparation of Precursor Solutions and Temperature Regulation

PM6 and L8-BO were dissolved in an appropriate solvent at a predetermined mass ratio to prepare the blend precursor solution, in which the donor-to-acceptor weight ratio was fixed at 1:1.3, with the donor and acceptor concentrations maintained at 4.5 and 5.85 mg mL^{-1}, respectively. To investigate the effect of initial temperature on precursor-solution assembly, subsequent film morphology, and device performance, the blend

solutions were adjusted to 50 °C, 60 °C, and 75 °C, respectively. The subsequent film deposition processes were then carried out under the corresponding temperature conditions to preserve the distinct molecular pre-aggregation states formed at different initial temperatures. The initial solution temperature can regulate the chain conformation, intermolecular interactions, and aggregation behavior of donor/acceptor molecules, thereby affecting the phase-separation evolution and molecular packing characteristics during film formation.

3. Absorption and Photoluminescence Measurements

To characterize the aggregation behavior of the precursor solutions at different temperatures, the UV-Vis-NIR absorption spectra and photoluminescence (PL) spectra of PM6, L8-BO, and PM6:L8-BO blend solutions were measured under different temperature conditions. By comparing the changes in absorption intensity and emission behavior, the influence of initial temperature on molecular pre-aggregation, local domain size, and donor/acceptor interfacial quenching was analyzed, providing a basis for understanding the subsequent film morphology regulation and device-performance enhancement.

4. Device Fabrication

Organic solar cells were fabricated with a conventional architecture of ITO/PEDOT:PSS/PM6:L8-BO/PFN-Br/Ag. The active-layer precursor solution was prepared by blending PM6 and L8-BO at a mass ratio of 1:1.3. To investigate the effect of the initial temperature on the liquid-state assembly behavior of the precursor solution and the subsequent evolution of film microstructure, the blend solutions were maintained at 50, 60, and 75 °C for 1 h, respectively, and then immediately used for device fabrication. Except for the initial temperature, all other processing conditions were kept identical.

Pre-cleaned ITO-coated glass substrates were first spin-coated with a PEDOT:PSS layer, followed by spin-coating of the PM6:L8-BO blend solution treated at different initial temperatures onto the PEDOT:PSS surface. The active layer was spin-coated at 4500 rpm for 30 s, yielding a film thickness of approximately 100 nm. The active layer was then thermally annealed at 100 °C for 5 min. Subsequently, PFN-Br was spin-

coated onto the active layer as the electron-transport layer, and finally, an Ag electrode was thermally evaporated to complete the device fabrication.

5. Film Morphology and Microstructure Characterization

To investigate the effect of initial temperature on the microstructure of the active layer, the PM6:L8-BO blend films were characterized using multiple morphological and structural techniques. Transmission electron microscopy (TEM) was used to analyze the phase-separation characteristics of the films. Atomic force microscopy (AFM) was employed to observe the surface morphology and determine the surface roughness. Grazing-incidence wide-angle X-ray scattering (GIWAXS) was used to study the molecular orientation, lamellar packing, and π-π stacking characteristics of the films. These measurements were performed to systematically reveal how liquid-state pre-assembly is translated into solid-state ordered structures under different temperature conditions.

6. Energy-Level Measurements

Cyclic voltammetry (CV) measurements combined with energy-level analysis were carried out to determine the frontier orbital energy levels of PM6 and L8-BO and to evaluate their energy-level alignment. The results were used to demonstrate that the donor/acceptor system possesses a suitable energy cascade, which is beneficial for exciton dissociation, charge separation, and selective charge transport.

7. Photovoltaic Performance Measurements

The current density-voltage (*J-V*) characteristics of the devices were measured under simulated AM 1.5G illumination at 100 mW cm^{-2}, and the corresponding photovoltaic parameters, including open-circuit voltage (V_{oc}), short-circuit current density (J_{sc}), fill factor (FF), and power conversion efficiency (PCE), were obtained. In addition, the external quantum efficiency (EQE) spectra were measured, and the integrated current densities were calculated from the EQE curves to verify the reliability of the J-V results.

8. Stability Tests

To evaluate the stability of devices prepared at different initial temperatures, photo-aging, storage-aging, and thermal-aging tests were conducted, and the performance decay of the devices was continuously monitored. By comparing the efficiency

retention of the devices over 500 h of aging, the influence of initial precursor-solution temperature on long-term device stability was assessed.

9. Charge-Transport and Recombination Characterization

To clarify the origin of the performance differences, charge-transport and recombination behaviors of the devices prepared under different conditions were systematically analyzed. The space-charge-limited current (SCLC) method was used to determine the hole and electron mobilities. Transient photocurrent (TPC) and transient photovoltage (TPV) measurements were performed to evaluate charge extraction and carrier recombination lifetimes. In addition, J_{ph}-V_{eff} curves, dark J-V measurements, steady-state PL, light-intensity-dependent measurements, and electrochemical impedance spectroscopy (EIS) were employed to comprehensively analyze exciton dissociation, charge generation, transport, extraction, and recombination processes.

10. Exciton Dynamics Characterization

Femtosecond transient absorption (TA) spectroscopy and time-resolved photoluminescence (TRPL) spectroscopy were conducted on PM6:L8-BO films prepared at different temperatures to investigate the excited-state dynamics. By analyzing the ground-state bleaching signals, kinetic decay curves, and lifetime variations, the influence of initial temperature on exciton dissociation efficiency, charge-generation stability, and non-radiative recombination losses was elucidated.

Supplementary Figures and Tables

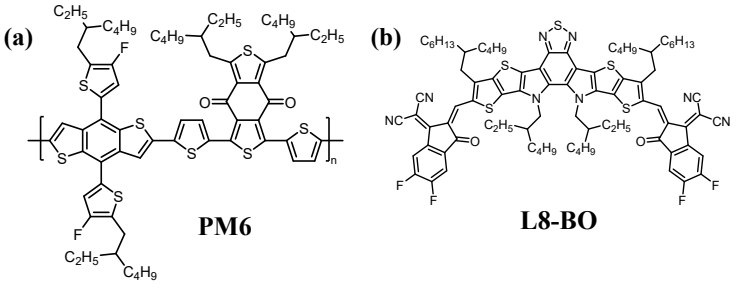

Figure S1. Molecular structures of (a) PM6 and (b) L8-BO.

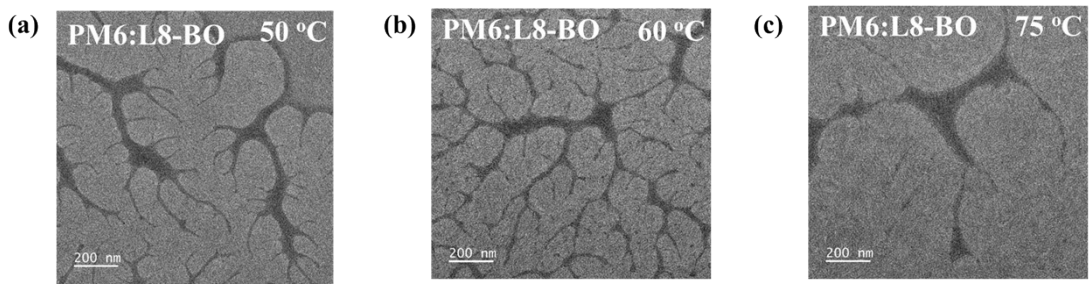

Figure S2. TEM images (a-c) of PM6:L8-BO films at different temperatures.

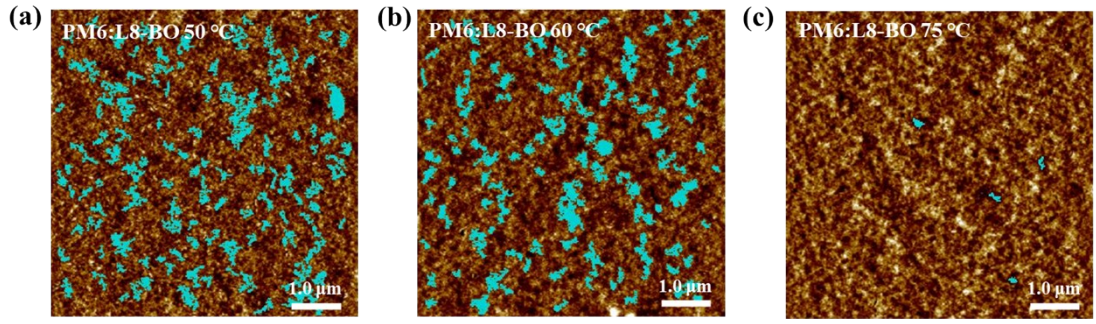

Figure S3. AFM height images (a-c) of PM6:L8-BO films at different temperatures.

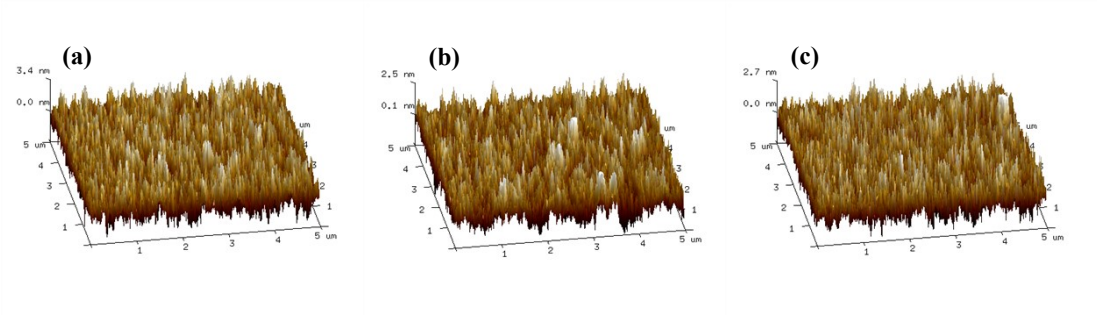

Figure S4. Three-dimensional AFM images of PM6:L8-BO thin films at different temperatures.

Table S1. Detailed GIWAXS (010) peak information in OOP of PM6:L8-BO films.

Film	Peak	Peak location ($Å^{-1}$)	π-π stacking distance (Å)	FWHM ($Å^{-1}$)	Lamellar stacking distance (nm)
PM6:L8-BO(50℃)	(010) in OOP	1.73	3.63	0.42	1.34
	(100) In IP	0.43	/	0.09	6.28

PM6:L8-BO(60℃)	(010) in OOP	1.74	3.61	0.45	1.25
	(100) In IP	0.44	/	0.08	7.06
PM6:L8-BO(75℃)	(010) in OOP	1.77	3.55	0.39	1.44
	(100) In IP	0.41	/	0.11	5.13

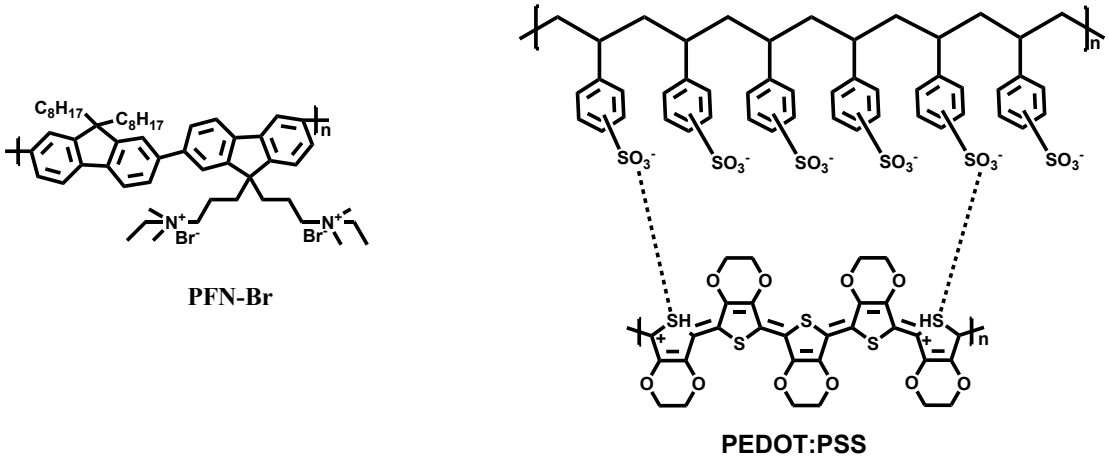

Figure S5. Molecular structures of PPFN-Br and PEDOT:PSS.

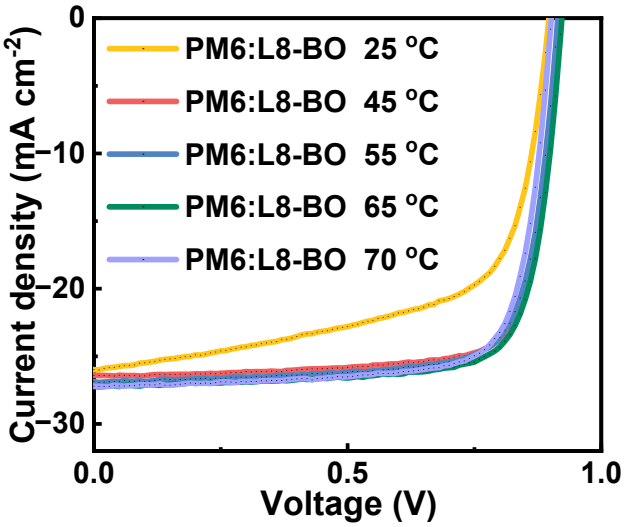

Figure S6. *J–V* characteristic curves of devices fabricated with PM6:L8-BO under different temperature conditions under AM 1.5G illumination.

Table S2. Photovoltaic parameters of PM6:L8-BO devices at different temperatures.

Devie	Temperature	V_{OC} (V)	J_{SC} [a] (mA cm^{-2})	FF (%)	PCE $_{avg}$ [b] (%)	PCE $_{max}$ (%)
PM6:L8-BO	25℃	0.89±0.01	25.37±0.38	63.72±0.46	14.67±0.13	14.80
	45℃	0.90±0.01	26.45±0.11	77.27±0.25	18.48±0.24	18.72
	55℃	0.90±0.01	27.24±0.28	79.24±0.57	19.26±0.31	19.57
	65℃	0.91±0.01	27.28±0.17	79.52±0.57	19.87±0.17	20.04
	70℃	0.90±0.01	27.33±0.25	79.01±0.24	19.13±0.35	19.48

Table S3. Photovoltaic parameters of OSCs with PM6:L8-BO ported in the literature.

Device	V_{OC} (V)	J_{SC} (mA cm^{-2})	FF (%)	PCE (%)	Ref.
PM6:L8-BO（o-XY）	0.875	26.20	79.40	18.20	1
PM6:L8-BO（DIM）	0.893	26.03	80.00	18.60	2
PM6:L8-BO（LbL）	0.880	26.97	77.64	18.43	3
PM6:L8-BO-X（CIPA）	0.896	27.65	79.70	19.74	4
PM6:L8-BO（5.2ᶜ）	0.888	25.70	79.90	18.20	5
PM6:L8-BO (SAA-LBL)	0.880	26.68	80.50	19.02	6
PM6:L8-BO (B3T)	0.891	27.78	79.82	19.75	7
PM6:L8-BO (90°C DIO)	0.881	26.56	78.33	18.33	8
PM6:L8-BO (Meso-LBL)	0.880	26.17	79.76	18.45	9
PM6:L8-BO	0.857	23.95	77.07	15.82	10
PM6:L8-BO (RT-cast)	0.890	26.10	76.70	17.70	11
PM6:L8-BO (S-SVA)	0.886	25.90	79.40	18.20	12
PM6:L8-BO	0.880	26.20	78.10	18.00	13

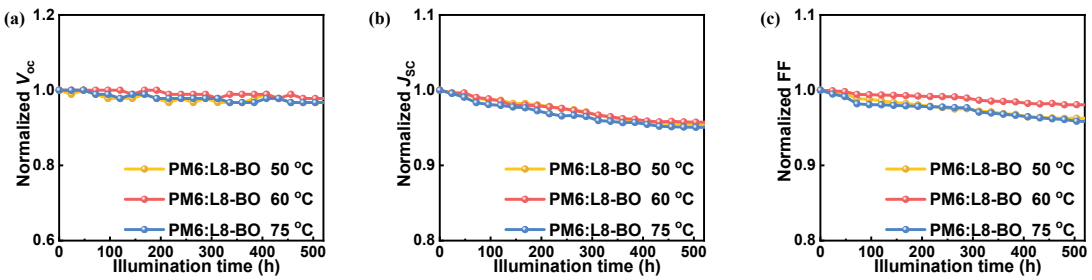

Figure S7. The optical stability of PM6:L8-BO devices.

Table S4. Photovoltaic parameters recorded for PM6:L8-BO devices fabricated at 50 °C under LED illumination at different time points.

	Illumination time (h)	V_{OC} (V)	J_{SC} (mA cm^{-2})	FF (%)	PCE (%)
50 °C	0	0.91	27.75	76.16	19.48
	24	0.90	27.66	75.42	19.16
	48	0.91	27.64	75.17	19.01
	72	0.90	27.45	74.81	18.45
	96	0.89	27.39	74.75	18.01
	120	0.89	27.38	74.78	18.05
	144	0.89	27.26	74.65	17.95
	168	0.90	27.26	74.67	17.99
	192	0.89	27.21	74.75	18.02
	216	0.88	27.15	74.61	17.92
	240	0.89	27.07	74.54	17.83
	264	0.88	27.03	74.52	17.81
	288	0.89	26.95	74.42	17.71
	312	0.88	26.81	74.11	17.51
	336	0.88	26.75	73.94	17.45
	360	0.88	26.64	73.81	17.38
	384	0.89	26.62	73.75	17.25
	408	0.90	26.58	73.59	17.12
	432	0.89	26.54	73.45	16.98
	456	0.88	26.52	73.42	16.91
	480	0.88	26.51	73.34	16.88
	504	0.88	26.49	73.25	16.85
	528	0.88	26.49	73.19	16.81

Table S5. Photovoltaic parameters recorded for PM6:L8-BO devices fabricated at 60 °C under LED illumination at different time points.

	Illumination time (h)	V_{OC} (V)	J_{SC} (mA cm^{-2})	FF (%)	PCE (%)
60 ℃	0	0.91	27.76	77.04	20.01
	24	0.91	27.65	76.98	19.89
	48	0.91	27.66	76.89	19.85
	72	0.91	27.49	76.61	19.61
	96	0.91	27.44	76.57	19.58
	120	0.91	27.36	76.55	19.51
	144	0.90	27.19	76.51	19.45
	168	0.91	27.21	76.48	19.46
	192	0.91	27.18	76.43	19.39
	216	0.90	27.14	76.39	19.36
	240	0.90	27.09	76.38	19.31
	264	0.90	27.01	76.36	19.28
	288	0.90	26.93	76.23	19.17
	312	0.89	26.84	76.01	19.01
	336	0.90	26.78	75.92	18.97
	360	0.90	26.71	75.89	18.95
	384	0.90	26.69	75.84	18.92
	408	0.90	26.62	75.69	18.87
	432	0.89	26.59	75.63	18.84
	456	0.90	26.61	75.68	18.79
	480	0.89	26.59	75.54	18.77
	504	0.89	26.58	75.55	18.76

	528	0.89	26.58	75.54	18.77

Table S6. Photovoltaic parameters recorded for PM6:L8-BO devices fabricated at 75 °C under LED illumination at different time points.

	Illumination time (h)	V_{OC} (V)	J_{SC} (mA cm^{-2})	FF (%)	PCE (%)
75 ℃	0	0.91	27.74	76.26	19.42
	24	0.91	27.62	75.87	19.15
	48	0.91	27.48	75.61	19.02
	72	0.90	27.28	74.88	18.39
	96	0.90	27.21	74.79	17.99
	120	0.89	27.18	74.78	18.01
	144	0.90	27.12	74.72	17.95
	168	0.90	27.09	74.67	17.89
	192	0.89	26.98	74.62	17.82
	216	0.89	26.87	74.58	17.75
	240	0.89	26.79	74.55	17.69
	264	0.89	26.81	74.49	17.65
	288	0.89	26.77	74.48	17.68
	312	0.89	26.62	74.03	17.53

	336	0.88	26.59	73.94	17.45
	360	0.88	26.54	73.82	17.36
	384	0.88	26.55	73.71	17.28
	408	0.89	26.48	73.57	17.14
	432	0.89	26.41	73.45	17.02
	456	0.88	26.39	73.36	16.97
	480	0.88	26.38	73.28	16.85
	504	0.88	26.37	73.11	16.71
	528	0.88	26.37	73.08	16.75

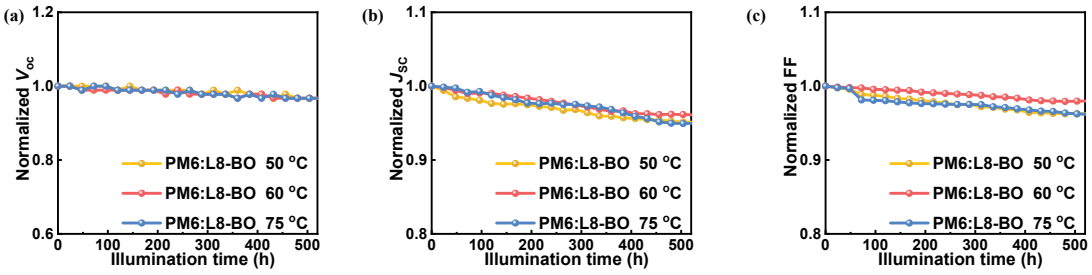

Figure S8. The storage stability of PM6:L8-BO devices.

Table S7. Photovoltaic parameters of PM6:L8-BO devices fabricated at 50 °C under storage with different time.

	Illumination time (h)	V_{OC} (V)	J_{SC} (mA cm^{-2})	FF (%)	PCE (%)
50 °C	0	0.91	27.77	76.44	19.59
	24	0.91	27.61	76.25	19.23
	48	0.91	27.37	76.11	18.92

	72	0.91	27.31	75.58	18.85
	96	0.91	27.24	75.51	18.67
	120	0.90	27.12	75.37	18.55
	144	0.91	27.09	75.18	18.38
	168	0.90	27.11	75.09	18.21
	192	0.90	27.07	74.95	18.11
	216	0.90	27.01	74.81	17.96
	240	0.90	26.97	74.68	17.78
	264	0.90	26.86	74.52	17.79
	288	0.89	26.89	74.55	17.77
	312	0.90	26.77	74.31	17.68
	336	0.89	26.65	74.24	17.62
	360	0.90	26.64	74.06	17.59
	384	0.89	26.58	73.98	17.51
	408	0.89	26.55	73.72	17.47
	432	0.88	26.51	73.68	17.38
	456	0.89	26.49	73.62	17.24
	480	0.88	26.45	73.58	17.11
	504	0.88	26.42	73.59	17.01
	528	0.88	26.41	73.58	16.96

Table S8. Photovoltaic parameters of PM6:L8-BO devices fabricated at 60 °C under storage with different time.

	Illumination time (h)	V_{OC} (V)	J_{SC} (mA cm^{-2})	FF (%)	PCE (%)
60 ℃	0	0.92	27.82	77.34	20.08
	24	0.92	27.77	77.24	19.91

48	0.91	27.66	77.19	19.81
72	0.91	27.54	77.15	19.83
96	0.91	27.56	77.01	19.74
120	0.91	27.55	76.97	19.75
144	0.91	27.48	76.91	19.76
168	0.91	27.43	76.88	19.64
192	0.91	27.37	76.71	19.52
216	0.90	27.31	76.64	19.47
240	0.91	27.25	76.58	19.44
264	0.90	27.18	76.51	19.45
288	0.90	27.11	76.45	19.43
312	0.90	27.03	76.38	19.35
336	0.90	26.95	76.23	19.21
360	0.89	26.87	76.19	19.18
384	0.90	26.89	76.08	19.12
408	0.90	26.78	75.89	19.05
432	0.89	26.78	75.81	19.01
456	0.89	26.75	75.78	19.02

	480	0.89	26.76	75.74	18.97
	504	0.89	26.75	75.77	18.95
	528	0.89	26.74	75.78	18.94

Table S9. Photovoltaic parameters of PM6:L8-BO devices fabricated at 75 °C under storage with different time.

	Illumination time (h)	V_{OC} (V)	J_{SC} (mA cm^{-2})	FF (%)	PCE (%)
75 ℃	0	0.91	27.65	75.97	19.05
	24	0.91	27.61	75.81	18.96
	48	0.90	27.58	75.73	18.85
	72	0.91	27.42	74.55	18.57
	96	0.91	27.45	74.51	18.41
	120	0.90	27.31	74.47	18.28
	144	0.90	27.22	74.35	18.17
	168	0.90	27.14	74.24	18.03
	192	0.90	27.02	74.18	17.91
	216	0.90	26.99	74.15	17.82
	240	0.89	27.01	74.11	17.68
	264	0.90	26.96	74.09	17.54
	288	0.89	26.97	74.09	17.42
	312	0.89	26.91	74.07	17.31
	336	0.89	26.87	73.85	17.23
	360	0.88	26.78	73.77	17.05
	384	0.89	26.65	73.64	16.86
	408	0.88	26.52	73.52	16.71
	432	0.89	26.44	73.41	16.66

	456	0.88	26.31	73.37	16.58
	480	0.88	26.26	73.21	16.60
	504	0.88	26.25	73.11	16.54
	528	0.88	26.26	73.08	16.53

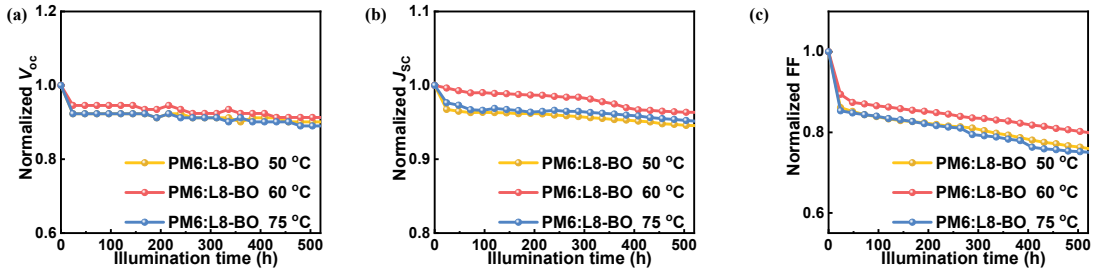

Figure S9. The thermal stability of PM6:L8-BO devices.

Table S10. Photovoltaic parameters of PM6:L8-BO devices fabricated at 50 °C under heating conditions with varying storage durations.

	Illumination time (h)	V_{OC} (V)	J_{SC} (mA cm^{-2})	FF (%)	PCE (%)
	0	0.91	27.65	76.12	19.02
	24	0.84	26.75	65.57	14.27
	48	0.84	26.68	64.85	14.03
50 °C	72	0.84	26.63	64.24	13.85
	96	0.84	26.64	63.87	13.77
	120	0.84	26.63	63.44	13.62
	144	0.84	26.62	63.12	13.58

168	0.84	26.59	62.94	13.42
192	0.83	26.60	62.69	13.29
216	0.84	26.58	62.38	13.11
240	0.84	26.54	62.09	12.88
264	0.83	26.51	61.94	12.73
288	0.83	26.48	61.71	12.65
312	0.83	26.44	61.22	12.48
336	0.83	26.41	60.73	12.31
360	0.82	26.37	60.38	12.13
384	0.83	26.35	59.89	12.01
408	0.83	26.31	59.43	11.87
432	0.83	26.28	59.01	11.68
456	0.82	26.21	58.74	11.53
480	0.82	26.19	58.36	11.45
504	0.82	26.15	58.09	11.31
528	0.82	26.14	57.72	11.25

Table S11. Photovoltaic parameters of PM6:L8-BO devices fabricated at 60 °C under heating conditions with varying storage durations.

	Illumination time (h)	V_{OC} (V)	J_{SC} (mA cm^{-2})	FF (%)	PCE (%)
	0	0.92	27.42	77.12	20.05
	24	0.87	27.32	68.98	18.13
	48	0.87	27.22	67.42	17.86
	72	0.87	27.14	67.13	17.62
	96	0.87	27.15	66.78	17.42
	120	0.87	27.12	66.54	17.26
	144	0.87	27.11	66.22	17.05
	168	0.86	27.08	65.92	16.87
	192	0.86	27.06	65.73	16.62
	216	0.87	27.05	65.47	16.47
	240	0.86	27.01	65.18	16.24
60 ℃	264	0.85	26.98	64.75	16.02
	288	0.85	26.98	64.46	15.86
	312	0.85	26.91	64.33	15.64
	336	0.86	26.81	64.05	15.32
	360	0.85	26.73	63.86	15.08
	384	0.85	26.59	63.45	14.83
	408	0.85	26.51	63.08	14.65
	432	0.84	26.49	62.85	14.48
	456	0.84	26.46	62.45	14.29
	480	0.84	26.44	62.19	14.15
	504	0.84	26.42	61.87	13.86
	528	0.84	26.42	61.57	13.72

Table S12. Photovoltaic parameters of PM6:L8-BO devices fabricated at 75 °C under heating conditions with varying storage durations.

	Illumination time (h)	V_{OC} (V)	J_{SC} (mA cm^{-2})	FF (%)	PCE (%)
	0	0.91	27.52	75.66	19.01
	24	0.84	26.87	64.58	14.58
	48	0.84	26.78	64.17	14.21
	72	0.84	26.61	63.85	13.97
	96	0.84	26.59	63.57	13.75
	120	0.84	26.66	63.12	13.52
	144	0.84	26.62	62.89	13.38
	168	0.84	26.58	62.56	13.15
	192	0.83	26.52	62.16	12.99
	216	0.84	26.55	61.79	12.72
	240	0.83	26.59	61.52	12.58
75 ℃	264	0.83	26.55	61.32	12.41
	288	0.83	26.55	60.11	12.28
	312	0.83	26.51	59.88	12.06
	336	0.82	26.48	59.65	11.89
	360	0.83	26.45	59.25	11.76
	384	0.82	26.41	58.98	11.58
	408	0.82	26.38	57.73	11.42
	432	0.82	26.32	57.43	11.28
	456	0.82	26.28	57.28	11.11
	480	0.81	26.25	57.01	11.08
	504	0.81	26.21	56.89	10.98
	528	0.81	26.18	56.75	10.82

Table S13. SCLC hole and electron mobility for PM6:L8-BO devices.

Device	Temperature	μ_h ($cm^2V^{-1}S^{-1}$)	μ_e ($cm^2V^{-1}S^{-1}$)	Thickness (nm)
PM6:L8-BO	50 ℃	1.64×10^{-3}	1.12×10^{-3}	~100
PM6:L8-BO	60 ℃	2.12×10^{-3}	1.52×10^{-3}	~100
PM6:L8-BO	75 ℃	1.54×10^{-3}	1.15×10^{-3}	~100

Table S14. Parameters related to the J_{ph}–V_{eff} curves calculated for PM6:L8-BO devices at different temperatures under AM 1.5G illumination.

Active layer [a]	Temperature	J_{ph} [b] (mA cm^{-2})	J_{sat} (mAcm^{-2})	G_{max} (m^{-3} s^{-1})	P(E, T)
PM6:L8-BO	50℃	25.59	26.84	1.67×10^{28}	0.953
	60℃	26.66	27.58	1.72×10^{28}	0.966
	75℃	25.51	26.74	1.67×10^{28}	0.954

Table S15. Photovoltaic parameters of D18:L8-BO devices at different temperatures.

Device	Temperature	V_{OC} (V)	J_{SC} [a] (mA cm^{-2})	$J_{SC,EQE}$ [b] (mA cm^{-2})	FF (%)	PCE $_{avg}$ [c] (%)	PCE $_{max}$ (%)
D18:L8-BO	50℃	0.90±0.01	27.03±0.29	26.24	78.95±0.26	19.42±0.25	19.67
	60℃	0.91±0.01	27.27±0.23	26.61	80.58±0.25	20.38±0.21	20.59
	75℃	0.90±0.01	26.94±0.31	26.36	78.24±0.37	19.23±0.31	19.54

Table S16. Photovoltaic parameters of PM6:Y6 devices at different temperatures.

Device	Temperature	V_{OC} (V)	J_{SC} [a] (mA cm^{-2})	$J_{SC,EQE}$ [b] (mA cm^{-2})	FF (%)	PCE $_{avg}$ [c] (%)	PCE $_{max}$ (%)
PM6:Y6	50℃	0.84±0.01	26.52±0.16	25.90	75.46±0.28	16.84±0.28	17.12
	60℃	0.86±0.01	26.88±0.27	26.16	76.72±0.13	17.65±0.29	17.94
	75℃	0.84±0.01	26.67±0.35	26.05	74.58±0.35	19.42±0.25	16.85

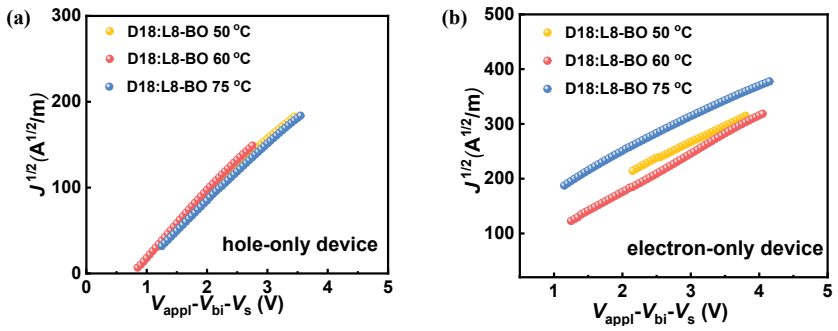

Figure S10 (a) SCLC hole mobility for D18:L8-BO at different temperatures. b SCLC electron mobility for D18:L8-BO at different temperatures.

Table S17. SCLC hole and electron mobility for D18:L8-BO devices.

Device	Temperature	μ_h ($cm^2V^{-1}S^{-1}$)	μ_e ($cm^2V^{-1}S^{-1}$)	Thickness (nm)
D18:L8-BO	50 °C	1.51×10^{-3}	1.21×10^{-3}	~100
D18:L8-BO	60 °C	1.92×10^{-3}	1.66×10^{-3}	~100
D18:L8-BO	75 °C	1.48×10^{-3}	1.32×10^{-3}	~100

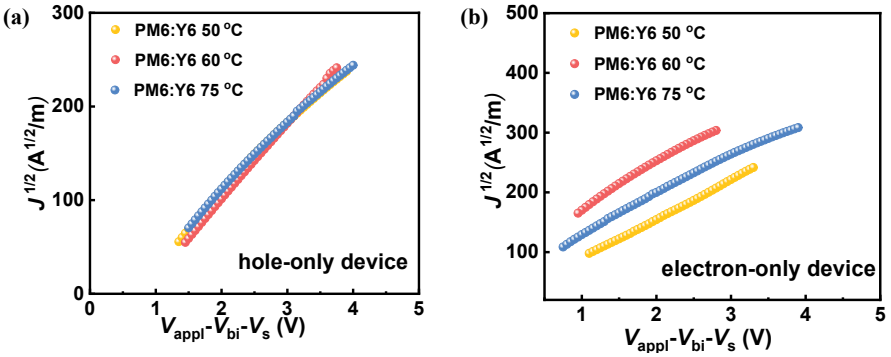

Figure S11 (a) SCLC hole mobility for PM6:Y6 at different temperatures. b SCLC electron mobility for PM6:Y6 at different temperatures.

Table S18. SCLC hole and electron mobility for PM6:Y6 devices.

Device	Temperature	μ_h ($cm^2V^{-1}S^{-1}$)	μ_e ($cm^2V^{-1}S^{-1}$)	Thickness (nm)
PM6:Y6	50 °C	1.69×10^{-3}	1.44×10^{-3}	~100
PM6:Y6	60 °C	2.18×10^{-3}	1.86×10^{-3}	~100

PM6:Y6	75 ℃	1.61×10^{-3}	1.36×10^{-3}	~100

References

1. E.-M. Feng, C.-J. Zhang, Y.-F. Han, J.-H. Chang, F. Yang, H.-Y. Li, Q. Luo, C.-Q. Ma, Y.-P. Zou, L.-M. Ding and J.-L. Yang, *J. Cent. South Univ.*, 2024, **31**, 4297-4306.

2. J. Song, L. Zhu, C. Li, J. Xu, H. Wu, X. Zhang, Y. Zhang, Z. Tang, F. Liu, Y. Sun, *Matter,* 2021, **7**, 2542-2552.

3. J. Zhang, W. Xu, H. Tian, Z. Liu, F. Zhang, *ChemPhotoChem*, 2024, **8**, e2023300348.

4. J. Zhang, X. Duan, X. Li, G. Dai, J. Dengn, X. Wang, J. Qiao, H. Wu, L. Liu, H. Huang, S. Liu, J. Yan, H. Zhang, X. Hao, R. Yang, F. Gao, Y. Sun, *Energy Environ, Sci.*, 2025, **18**, 5378-5388.

5. L. Zhu, M. Zhang, J. Xu, C. Li, J. Yan, G. Zhou, W. Zhong, T. Hao, J. Song, X. Xue, Z. Zhou, R. Zeng, H. Zhu, C.-C. Chen, R. C. I. MacKenzie, Y. Zou, J. Nelson, Y. Zhang, Y. Sun, F. Liu, *Nat. Mater*., 2022, **21**, 522–530.

6. G. Ding, T. Chen, M. Wang, X. Xia, C. He, X. Zheng, Y. Li, D. Zhou, X. Lu, L. Zuo, Z. Xu, H. Chen, *Nano-Micro Lett*. 2023, **15**, 92.

7. D. Wu, J. Peng, Y. Zhong, H. Guo, J. Zhou, L. Ye, J. Zhang, K. Han, H. Liu, X. Lu, M. Huang, *Chem. Eng. J.* 2025, **524**, 168963.

8. Y. Li, B. Wang, L. Chen, Y. Yuan, J. Fu, C. Geng, J. Wan, H.-Q. Wang, *Phys. Chem. Chem. Phys.* 2025, **27**, 301.

9. C. Xie, H. Huang, Z. Li, X. Zeng, B. Deng, C. Li, G. Zhang, S. Li, *Polymers*, 2023. **16**, 91.

10. X. Li,, H. Yang, X. Du, H. Lin, G. Yang, C. Zheng, S. Tao, *Chem. Eng. J.*, 2023, **474**, 145782.

11. J. Cheng, C. Guo, L. Wang, D. Liu, W. Li, T. Wang, et al. *Joule*, 2024, **8**, 2250–2264.

12. S. Guo, C. Yan, H. Li, J. Zhu, Y. Zheng, Q. Qi, X. Yan, H. Yu, Y. Gong, J. Wang, J. Qimn, L. Meng, Y. Chen, Y. Li. P. Cheng, *J. Energy Chem.* 2025, **104**, 397-403.

13. B. Cheng, W. Hou, C. Han, S. Cheng, X. Xia, X. Guo, Y. Li, M. Zhang, *Energy Environ, Sci.*, 2025, **18**, 1375-1384.